Available online at www.sciencedirect.com
ScienceDirect
International Journal of Multiphase Flow 34 (2008) 647–664
International Journal of Multiphase Flow
www.elsevier.com/locate/ijmulflow

Nonlinear instability of an annular liquid sheet exposed to gas flow

A.A. Ibrahim, M.A. Jog *

Department of Mechanical, Industrial, and Nuclear Engineering, 598 Rhodes Hall, P.O. Box 210072, University of Cincinnati, Cincinnati, OH 45221, United States

Received 26 January 2007; received in revised form 31 July 2007

Abstract

Nonlinear instability and breakup of an annular liquid sheet has been modeled in this paper. The liquid sheet is considered to move axially and is exposed to co-flowing inner and outer gas streams. Also, the effect of outer gas swirl on sheet breakup has been studied. In the developed model a perturbation expansion method has been used with the initial magnitude of the disturbance as the perturbation parameter. This is a comprehensive model in that other geometries of planar sheet and a coaxial jet can be obtained as limiting cases of very large inner radius and inner radius equal to zero, respectively. In this temporal analysis, the effect of liquid Weber number, initial disturbance amplitude, inner gas-to-liquid velocity ratio, outer gas-to-liquid velocity ratio and outer gas swirl strength on the breakup time is investigated. The model is validated by comparison with earlier analytical studies for the limiting case of a planar sheet as well as with experimental data of sheet breakup length available in literature. It is shown that the linear theory cannot predict breakup of an annular sheet and the developed nonlinear model is necessary to accurately determine the breakup length. In the limiting case of a coaxial jet, results show that gas swirl destabilizes the jet, makes helical modes dominant compared to the axisymmetric mode and decreases jet breakup length. These results contradict earlier linear analyses and agree with experimental observations. For an annular sheet, it is found that gas flow hastens the sheet breakup process and shorter breakup lengths are obtained by increasing the inner and the outer gas velocity. Axially moving inner gas stream is more effective in disintegrating the annular sheet compared to axially moving outer gas stream. When both gas streams are moving axially, the liquid sheet breakup is quicker compared to that with any one gas stream. In the absence of outer gas swirl, the axisymmetric mode is the dominant instability mode. However, when outer gas flow has a swirl component higher helical modes become dominant. With increasing outer gas swirl strength, the maximum disturbance growth rate increases and the most unstable circumferential wave number increases resulting in a highly asymmetric sheet breakup with shorter breakup lengths and thinner ligaments.

Keywords: Atomization; Instability; Sheet breakup

1. Introduction

Atomization of an annular liquid sheet aided by co-flowing air streams is encountered in many spray and coating applications. For example, in airblast atomizers used in fuel injection systems for gas turbine engines, fuel is first forced into an annular passage to form a thin annular sheet, and it is then exposed to moving air streams on both sides. The strong shear action of moving air streams speeds up the disintegration process of the liquid sheet. A significant advantage of such atomizers over pressure atomizers is that airblast atomizers can produce fine sprays even at low liquid flow rates. Swirl may be added to the outer air stream to improve atomization and mixing. However, the process of sheet breakup in the presence of swirling air stream is not well understood (Lefebvre, 1980, 1983). To analyze and simulate spray systems, it is important to

* Corresponding author. Tel.: +1 513 556 1675; fax: +1 513 556 3390.
E-mail address: Milind.Jog@uc.edu (M.A. Jog).

0301-9322/$ - see front matter © 2008 Elsevier Ltd. All rights reserved.
doi:10.1016/j.ijmultiphaseflow.2007.12.003

develop predictive models for sheet breakup process in the presence of air flow so that the breakup length and the resulting droplet diameter can be determined.

Several experimental investigations of annular sheet breakup are available where effect of air flow has been studied (Shen, 1997; Carvalho and Heitor, 1998; Chin et al., 2000 and Adzic et al., 2001). Adzic et al. (2001) have investigated the disintegration of an annular liquid sheet in a coaxial airblast injector at low atomizing air velocities using optical methods. They have demonstrated that the breakup length of the annular liquid sheet is a function of the sum of the inner and outer air momentum of the coaxial air flows ($L_b \propto ({U_{\text{inner}}}^2 + {U_{\text{outer}}}^2)^{-0.44}$). This appears to be somewhat different from a circular liquid jet or a planar sheet breakup in co-flowing air where the effect of co-flowing gas is often introduced in terms of relative velocity (for example, $L_b \propto (U_R^2)^{-0.4}$ for liquid jet (Eroglu et al., 1991) and $L_b \propto (U_R^2)^{-0.5}$ for planar liquid sheet (Arai and Hashimoto, 1985)). However, it is likely that due to the low liquid velocities used by Adzic et al. (2001), the difference in gas absolute velocity and relative velocity may be quite small. Carvalho and Heitor (1998) have studied experimentally the atomization process of an annular liquid sheet in an axisymmetric shear layer formed through the interaction of turbulent coaxial jets (respectively, inner and outer jets), with and without swirl, in a model prefilming airblast atomizer. Both axial inner air flow and axial outer air flow were found to decrease the breakup length. However, the influence of axial inner air flow was much stronger ($L_b \propto ({U_{\text{inner}}}^2)^{-0.5}$) than a nearly linear dependence of outer air flow ($L_b \propto \text{constant} - 0.57 U_{\text{outer}}$). However, they have reported that the effect of outer air in destabilizing the sheet becomes significantly stronger when swirl is imparted to the outer air and it grows as the swirl strength is increased. Shen (1997) has carried out measurements of breakup length and drop size distribution for an annular sheet breakup in inner and outer air streams. His work confirms that co-flowing air streams hasten sheet breakup. His drop size measurements show that the drop distribution is narrower with air flow compared to that without co-flowing inner and outer air streams.

It is well known that the growth of disturbances on liquid sheet leads to sheet instability and breakup. Linear stability analyses are available in the literature that cover a wide range of configurations i.e. inviscid annular sheet moving axially with axial gas flow (Liao et al., 2000b), and swirling liquid sheet (Ponstein, 1959), with swirling gas flow (Panchagnula et al., 1996; Ibrahim and Jog, 2006), axially moving viscous liquid sheet subjected to axially moving inner and outer gas stream at different velocities (Shen and Li, 1996; Cao, 2003; Jeandel and Dumouchel, 1999), viscous liquid sheet in swirling gas streams (Liao et al., 2001; Du and Li, 2005), and a non-Newtonian annular liquid sheet (Alleborn et al., 1998). A comprehensive review of linear instability theories for liquid sheets and jets is given by Lefebvre (1989), Sirignano and Mehring (2000), Lin (2003), Yoon and Heister (2003) and recently by Ibrahim and Jog (2006). Unfortunately, the underlying assumption of infinitesimal disturbance magnitude limits the applicability of linear theory to the onset of sheet instability. The solutions become inapplicable as the perturbation amplitude grows and causes sheet breakup. As such, to accurately predict sheet evolution and breakup, a nonlinear treatment is necessary. Furthermore, it has been shown that at high Weber numbers and for gas-to-liquid density ratio of less than about 0.1 (conditions prevalent in most spray systems), the para-sinuous mode is the dominant disturbance growth pattern. Even if we were to extend the linear analysis to large deformations, for the para-sinuous mode linear theory would predict that the two interfaces remain parallel as they deform. Therefore, in the atomization literature, an empirical sheet breakup criterion has been used with the linear analysis, where sheet is considered to breakup when the disturbance grows by a factor of e^{12} (Clark and Dombrowski, 1972). Although this criterion has been applied in spray modeling (Schmidt et al., 2003), detailed experimental measurements of Blaisot and Adeline (2000, 2003) reveal that at breakup the growth of the disturbance can vary by orders of magnitude from e^{12}.

Few nonlinear analyses of thin annular liquid sheet breakup have been reported (Lee and Wang, 1986; Panchagnula et al., 1998; Mehring and Sirignano, 1999a,b and Park and Heister, 2006) but none of these consider the effect of gas flow on sheet breakup. Lee and Wang (1986) have developed a model for the dynamic formation of spherical shells from an annular inviscid membranes issuing from a nozzle and treated the liquid layer as a membrane moving under the influence of its own inertia, surface tension and gaseous hydrostatic pressure difference between its two sides. They have assumed that the liquid layer has zero thickness with no structure (internal flow) but with finite inertia which is subjected to change due to stretching and relaxing of the sheet during motion. Panchagnula et al. (1998) have developed a nonlinear model of annular liquid sheet using approximate one-dimensional equations derived by thin sheet approximations. They have considered only the para-varicose disturbances and have neglected the aerodynamic effects of the gas phase inside and outside the liquid sheet. It has been reported in the earlier studies (Shen and Li, 1996 and Ibrahim et al., 2006) that the para-varicose disturbances dominate the breakup process at very low liquid Weber numbers. In most practical atomizers, liquid Weber numbers are generally high and the para-sinuous disturbances dominate the breakup process in this regime. Mehring and Sirignano (1999a,b) have developed nonlinear models of axisymmetric thin inviscid infinite (periodically disturbed) and semi-infinite (locally forced) annular liquid sheets in a surrounding void with non-zero gas core pressure at zero gravity by employing a reduced dimension approach (long-wavelength approximation). Nonlinear breakup of a planar sheet has been investigated by Jazayeri and Li (2000) using a perturbation scheme, and numerically by Tharakan et al. (2002). Heister and co-workers have used the boundary element method to model the nonlinear stability of liquid jet (Yoon and Heister, 2004; Park et al., 2006) and of a conical sheet (Park and Heister, 2006). Their results agree with jet/sheet breakup in stagnant gaseous medium.

The main objective of this paper is to develop a nonlinear instability model for an annular liquid sheet subjected to unequal inner and outer gas velocities including outer gas swirl. Our development is new and comprehensive in that earlier work (linear and nonlinear) can be recovered as limiting cases of our development. In the limit of inner radius equal to zero, a solution for the jet can be obtained. In the limit of inner radius going to infinity (keeping sheet thickness constant), planar sheet behavior can be predicted. The developed model is used to study the effect of liquid Weber number, inner gas-to-liquid velocity ratio, outer gas-to-liquid velocity ratio, and the outer gas swirl velocity ratio, on sheet instability, deformation, and breakup.

2. Mathematical formulation

An annular liquid sheet of thickness "h" is considered as shown in Fig. 1. Mean flows of the inner gas, liquid and the outer gas are assumed to be $(U_1,0,0)$, $(U_2,0,0)$, and $(U_3,0,W_3=A_o/r)$, respectively. The densities of the inner, liquid and outer gas phases are ρ_1, ρ_2 and ρ_3, respectively. The effect of gravity is neglected because the Froude number (defined as the ratio of liquid inertia to gravity) is typically very large for practical sprays. Both phases are assumed to be incompressible. In the present formulation, liquid and gas flows are assumed to be inviscid and irrotational. Therefore, the entire flow field can be treated as a potential flow (White, 1991). At high Weber number, viscosity has been shown to have a small stabilizing effect on an annular sheet (Liao et al., 2001). As such, to keep the problem mathematically tractable, we have neglected viscosity in both phases. Liao et al. (2001) have shown that the difference in growth rate between an annular viscous sheet and an inviscid sheet becomes negligible for Reynolds number greater than about 100. Also, Cousin and Dumouchel (1996) and later Jeandel and Dumouchel (1999) have shown for planar sheet and annular sheet, respectively, that when We_G^2/Re is below 10^{-3}, the effect of viscosity can be neglected. Here We_G is the Weber number based on gas density $We_G=\frac{\rho_{\mathrm{Gas}}U_{\mathrm{liquid}}^2 h}{\sigma}$. These conditions are met in most atomization applications. For example, a sheet of water of 1 mm thickness moving with 10 m/s velocity will have Reynolds number of order 10^4 and $We_G^2/Re<10^{-3}$.

When the base flow, described above, is perturbed by a small disturbance, the two liquid–gas interfaces are displaced to new locations denoted by $r_a=a+\eta_a$ and $r_b=b+\eta_b$. All the physical parameters are non-dimensionalized such that length, time and density are scaled with sheet thickness h, the convection time h/U_2 and the liquid density ρ_2. The dimensionless surface deformation η_a and η_b and the velocity potential ϕ for the liquid and the gas phases must satisfy the following mass conservation equations:

$$\nabla\phi_j^2=0,\quad j=\mathrm{L}\ (r_a\leqslant r\leqslant r_b);\ \ j=\mathrm{i}\ (0\leqslant r\leqslant r_a);\ \ j=\mathrm{o}\ (r_b\leqslant r). \tag{1}$$

The subscripts L, i, and o indicate liquid, inner gas flow, and outer gas flow, respectively. The interface boundary conditions are

Kinematic conditions for liquid, inner gas, and outer gas are

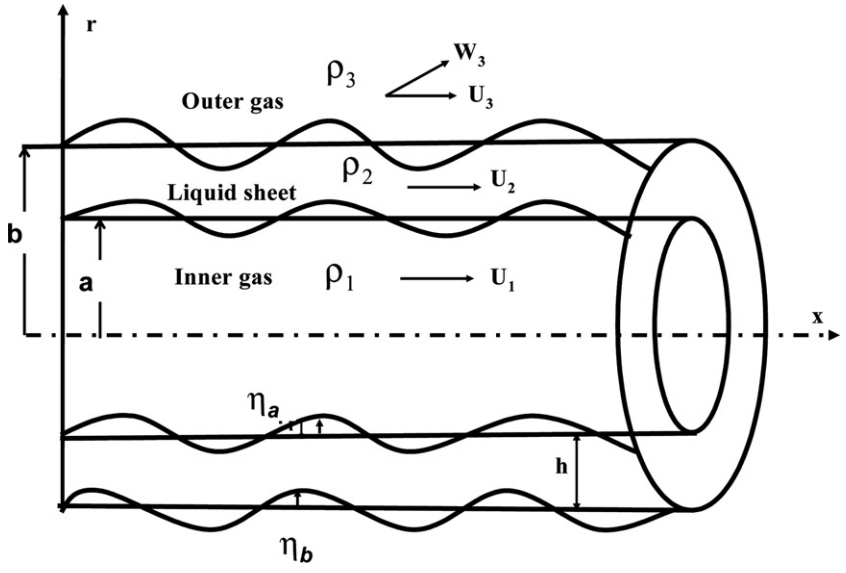

Fig. 1. A schematic of annular liquid sheet.

$$\phi_{\mathrm{L}a,r} - \eta_{a,t} + \phi_{\mathrm{L}a,x}\eta_{a,x} = 0 \quad \text{at } r_a, \tag{2}$$

$$\phi_{\mathrm{L}b,r} - \eta_{b,t} + \phi_{\mathrm{L}b,x}\eta_{b,x} = 0 \quad \text{at } r_b, \tag{3}$$

$$\phi_{\mathrm{i},r} - \eta_{a,t} + \phi_{\mathrm{i},x}\eta_{a,x} = 0 \quad \text{at } r_a, \tag{4}$$

$$\phi_{\mathrm{o},r} - \eta_{b,t} + \phi_{\mathrm{o},x}\eta_{a,x} + \frac{\phi_{\mathrm{o},\theta}\eta_{a,\theta}}{r^2} = 0 \quad \text{at } r_b. \tag{5}$$

The force balance conditions at the two interfaces called are the dynamic boundary conditions. At $r = r_a$:

$$\frac{1}{2} - \frac{1}{2}g_{\mathrm{i}}U_{\mathrm{i}}^2 + g_{\mathrm{i}}\phi_{\mathrm{i},t} - \phi_{\mathrm{L},t} + \frac{1}{2}g_{\mathrm{i}}\nabla\phi_{\mathrm{i}}^2 - \frac{1}{2}\nabla\phi_{\mathrm{L}}^2 = \frac{-1}{We_{\mathrm{L}}}\left(1 + \frac{\eta_{a\theta}^2}{r^2} + \eta_{ax}^2\right)^{-\frac{3}{2}}\left\{\frac{1}{r}\left(1 + \frac{2\eta_{a\theta}^2}{r^2} + \eta_{ax}^2\right) - \frac{1+\eta_{ax}^2}{r^2}\eta_{a\theta\theta} - \left(1 + \frac{\eta_{a\theta}^2}{r^2}\right)\eta_{axx} + \frac{2\eta_{ax}\eta_{a\theta}\eta_{ax\theta}}{r^2}\right\} + \frac{1}{We_{\mathrm{L}}a}. \tag{6}$$

At $r = r_b$

$$\frac{1}{2} - \frac{1}{2}g_{\mathrm{o}}\frac{W_{\mathrm{o}}^2}{b^2} - \frac{1}{2}g_{\mathrm{o}}U_{\mathrm{o}}^2 + g_{\mathrm{o}}\phi_{\mathrm{o},t} - \phi_{\mathrm{L},t} + \frac{1}{2}g_{\mathrm{o}}\nabla\phi_{\mathrm{o}}^2 - \frac{1}{2}\nabla\phi_{\mathrm{L}}^2 = \frac{1}{We_{\mathrm{L}}}\left(1 + \frac{\eta_{b\theta}^2}{r^2} + \eta_{bx}^2\right)^{-\frac{3}{2}}\left\{\frac{1}{r}\left(1 + \frac{2\eta_{b\theta}^2}{r^2} + \eta_{bx}^2\right) - \frac{1+\eta_{bx}^2}{r^2}\eta_{b\theta\theta} - \left(1 + \frac{\eta_{b\theta}^2}{r^2}\right)\eta_{bxx} + \frac{2\eta_{bx}\eta_{b\theta}\eta_{bx\theta}}{r^2}\right\} - \frac{1}{We_{\mathrm{L}}b}. \tag{7}$$

In the above equations, the subscript x, r, t, θ indicate derivatives with respect to x, r, t, and θ, respectively. The dimensionless liquid Weber number We_{L}, and inner gas velocity ratio (U_{i}), outer gas velocity ratio (U_{o}), inner density ratio g_{i} and outer density ratio g_{o} are defined as

$$We_{\mathrm{L}} = \frac{\rho_2 U_2^2 h}{\sigma}, \quad U_{\mathrm{i}} = \frac{U_1}{U_2}, \quad U_{\mathrm{o}} = \frac{U_3}{U_2}, \quad W_{\mathrm{o}} = \frac{A_{\mathrm{o}}}{hU_2}, \quad g_{\mathrm{i}} = \frac{\rho_1}{\rho_2} \text{ and } g_{\mathrm{o}} = \frac{\rho_3}{\rho_2}.$$

To obtain a solution for η_a and η_b regular perturbation theory is utilized with the initial disturbance amplitude η_{o} as the perturbation parameter. This is similar to the method used by Clark and Dombrowski (1972) for a planar sheet breakup in stagnant medium. However, unlike a planar sheet, the two interfaces for an annular sheet have different curvature and the geometry is not symmetric. Furthermore, consideration of different velocities for the inner and outer gas stream and outer gas swirl make the development presented here enormously more laborious and complex compared to that of Clark and Dombrowski (1972). We note that earlier linear and nonlinear analyses by perturbation method for a planar sheet and a coaxial jet can be recovered as limiting cases of the model presented here. By means of series expansion method under the perturbation scheme, the surface deformations or the location of the two liquid gas interfaces are expanded in power series of η_{o} as

$$\eta_a(x,\theta,t) = \sum_{n=1}^{n=\infty} \eta_{\mathrm{o}}^n \eta_{a,n}(x,\theta,t), \tag{8}$$

$$\eta_b(x,\theta,t) = \sum_{n=1}^{n=\infty} \eta_{\mathrm{o}}^n \eta_{b,n}(x,\theta,t). \tag{9}$$

The term η_{o}^0 is neglected from the expansion since it corresponds to the unperturbed interfaces, which are known. Assuming that $\eta_{a,\,n}$ and $\eta_{b,n}$ and all its derivatives are of the same order of magnitude, the forms of the kinematic boundary conditions suggest that the velocity potentials for the liquid and the gas phases can also be expanded in power series of η_{o} as

$$\phi_j(x,r,\theta,t) = \sum_{n=0}^{n=\infty} \eta_{\mathrm{o}}^n \phi_{j,n}(x,r,\theta,t), \quad j = \mathrm{L},\mathrm{i},\mathrm{o}, \tag{10}$$

where $\phi_{\mathrm{L},0} = x$, $\phi_{\mathrm{i},0} = U_{\mathrm{i}}x$ and $\phi_{\mathrm{o},0} = U_{\mathrm{o}}x + W_{\mathrm{o}}\theta$ represent the base flow field.

Since the governing equations (Eq. (1)) are linear, by applying the principle of superposition, each of the velocity potentials ($\phi_{\mathrm{L},n}$, $\phi_{\mathrm{i},n}$, and $\phi_{\mathrm{o},n}$) must satisfy the governing equations independently. The corresponding boundary conditions are obtained by substituting Eq. (10) into Eqs. (2)–(7), and equating to zero the successive coefficients of the same power of η_{o}^n. Under such a scheme, the velocity potentials need to be evaluated at the disturbed interfaces which are part of the solution and not known a priori. To overcome this difficulty,$\phi_{\mathrm{L},n}$, $\phi_{\mathrm{i},n}$ and $\phi_{\mathrm{o},n}$ are approximated by a Taylor series expansion around the unperturbed interfaces. The governing equations and the corresponding boundary conditions thus obtained for the first and the second order are obtained and are:

First-order (η_o):

$$\nabla\phi_{j1}^2 = 0, \quad j = \mathrm{L}\ (r_a \leqslant r \leqslant r_b);\ \ j = \mathrm{i}\ (0 \leqslant r \leqslant r_a);\ \ j = \mathrm{o}(r_b \leqslant r). \tag{11}$$

Interface conditions:

$$\phi_{\mathrm{L}1,r} - \eta_{a1,t} + \eta_{a1,x} = 0 \quad \text{at } a, \tag{12}$$

$$\phi_{\mathrm{L}1,r} - \eta_{b1,t} + \eta_{b1,x} = 0 \quad \text{at } b, \tag{13}$$

$$\phi_{\mathrm{i}1,r} - \eta_{a1,t} + U_\mathrm{i}\eta_{a1,x} = 0 \quad \text{at } a, \tag{14}$$

$$\phi_{\mathrm{o}1,r} - \eta_{b1,t} + U_\mathrm{o}\eta_{b1,x} + \frac{W_\mathrm{o}}{b^2}\eta_{b1,\theta} = 0 \quad \text{at } b, \tag{15}$$

$$g_\mathrm{i}\phi_{\mathrm{i}1,t} - \phi_{\mathrm{L}1,t} + g_\mathrm{i}U_\mathrm{i}\phi_{\mathrm{i}1,x} - \phi_{\mathrm{L}1,x} = \frac{1}{We_\mathrm{L}}\left(\frac{\eta_{a1} + \eta_{a1,\theta\theta}}{a^2} + \eta_{a1,xx}\right) \quad \text{at } a, \tag{16}$$

$$g_\mathrm{o}\phi_{\mathrm{o}1,t} - \phi_{\mathrm{L}1,t} + g_\mathrm{o}U_\mathrm{o}\phi_{\mathrm{o}1,x} + g_\mathrm{o}\frac{W_\mathrm{o}}{b^2}\phi_{\mathrm{o}1,\theta} - \phi_{\mathrm{L}1,x} = \frac{-1}{We_\mathrm{L}}\left(\frac{\eta_{b1} + \eta_{b1,\theta\theta}}{b^2} + \eta_{b1,xx}\right) + g_\mathrm{o}\frac{W_\mathrm{o}^2}{b^3}\eta_{b1} \quad \text{at } b. \tag{17}$$

Initial conditions:

$$\eta_{a1}(x,\theta,0) = \cos(kx + n\theta) \quad \text{and} \quad \eta_{a1,t}(x,\theta,0) = 0, \tag{18}$$

$$\eta_{b1}(x,\theta,0) = \cos(kx + n\theta) \quad \text{and} \quad \eta_{b1,t}(x,\theta,0) = 0. \tag{19}$$

Here k is the axial wave number and n is the circumferential wave number.

Second-order (η_o^2):

$$\nabla\phi_{\mathrm{L}2}^2 = 0, \quad j = \mathrm{L}\ (r_a \leqslant r \leqslant r_b);\ \ j = \mathrm{i}\ (0 \leqslant r \leqslant r_a);\ \ j = \mathrm{o}(r_b \leqslant r). \tag{20}$$

Interface conditions:

$$\phi_{\mathrm{L}2,r} - \eta_{a2,t} - \eta_{a2,x} = \eta_{a1,x}\phi_{\mathrm{L}1,x} + \frac{\eta_{a1}\eta_{a1,\theta}}{a^2} - \eta_{a1}\phi_{\mathrm{L}1,rr} \quad \text{at } a, \tag{21}$$

$$\phi_{\mathrm{L}2,r} - \eta_{b2,t} - \eta_{b2,x} = \eta_{b1,x}\phi_{\mathrm{L}1,x} + \frac{\eta_{b1}\eta_{b1,\theta}}{b^2} - \eta_{b1}\phi_{\mathrm{L}1,rr} \quad \text{at } b, \tag{22}$$

$$\phi_{\mathrm{i}2,r} - \eta_{a2,t} - U_\mathrm{i}\eta_{a2,x} = \eta_{a1,x}\phi_{\mathrm{i}1,x} + \frac{\eta_{a1}\eta_{a1,\theta}}{a^2} - \eta_{a1}\phi_{\mathrm{i}1,rr} \quad \text{at } a, \tag{23}$$

$$\phi_{\mathrm{o}2,r} - \eta_{a2,t} - U_\mathrm{o}\eta_{a2,x} - \frac{W_\mathrm{o}}{b^2}\eta_{a2,\theta} = \eta_{a1,x}\phi_{\mathrm{o}1,x} + \frac{\eta_{a1}\eta_{a1,\theta}}{b^2} - \eta_{a1}\phi_{\mathrm{o}1,rr} - \frac{2W_\mathrm{o}}{b^3}\eta_{a1}\eta_{a1,\theta} \quad \text{at } b, \tag{24}$$

$$\begin{aligned}
&g_\mathrm{i}\phi_{\mathrm{i}2,t} - \phi_{\mathrm{L}2,t} + g_\mathrm{i}U_\mathrm{i}\phi_{\mathrm{i}2,x} - \phi_{\mathrm{L}2,x} - \frac{1}{We_\mathrm{L}}\left(\frac{\eta_{a2} + \eta_{a2,\theta\theta}}{a^2} + \eta_{a2,xx}\right) \\
&\quad = (\eta_{a1,t}\phi_{\mathrm{L}1,r} + \eta_{a1}\phi_{\mathrm{L}1,rt}) - g_\mathrm{i}(\eta_{a1,t}\phi_{\mathrm{i}1,r} + \eta_{a1}\phi_{\mathrm{i}1,rt}) + (\eta_{a1,x}\phi_{\mathrm{L}1,r} + \eta_{a1}\phi_{\mathrm{L}1,rx}) - g_\mathrm{i}U_\mathrm{i}(\eta_{a1,x}\phi_{\mathrm{i}1,r} + \eta_{a1}\phi_{\mathrm{i}1,rx}) \\
&\qquad + \frac{1}{2}\left(\phi_{\mathrm{L}1,x}^2 + \phi_{\mathrm{L}1,r}^2 + \frac{\phi_{\mathrm{L}1,\theta}^2}{a^2}\right) - \frac{1}{2}g_\mathrm{i}\left(\phi_{\mathrm{i}1,x}^2 + \phi_{\mathrm{i}1,r}^2 + \frac{\phi_{\mathrm{i}1,\theta}^2}{a^2}\right) + \frac{(2\eta_{a1}^2 + 4\eta_{a1}\eta_{a1,\theta\theta} - \eta_{a1,\theta}^2 - a^2\eta_{a1,x}^2)}{2We_\mathrm{L}a^3} \quad \text{at } a,
\end{aligned} \tag{25}$$

$$\begin{aligned}
&g_\mathrm{o}\phi_{\mathrm{o}2,t} - \phi_{\mathrm{L}2,t} + g_\mathrm{o}U_\mathrm{o}\phi_{\mathrm{o}2,x} + g_\mathrm{o}\frac{W_\mathrm{o}}{b^2}\phi_{\mathrm{o}2,\theta} - \phi_{\mathrm{L}2,x} + \frac{1}{We_\mathrm{L}}\left(\frac{\eta_{b2} + \eta_{b2,\theta\theta}}{b^2} + \eta_{b2,xx}\right) - g_\mathrm{o}\frac{W_\mathrm{o}^2}{b^3}\eta_{b2} \\
&\quad = (\eta_{b1,t}\phi_{\mathrm{L}1,r} + \eta_{b1}\phi_{\mathrm{L}1,rt}) - g_\mathrm{o}(\eta_{b1,t}\phi_{\mathrm{o}1,r} + \eta_{b1}\phi_{\mathrm{o}1,rt}) + (\eta_{b1,x}\phi_{\mathrm{L}1,r} + \eta_{b1}\phi_{\mathrm{L}1,rx}) \\
&\qquad - g_\mathrm{o}U_\mathrm{o}(\eta_{b1,x}\phi_{\mathrm{o}1,r} + \eta_{b1}\phi_{\mathrm{o}1,rx}) - g_\mathrm{o}\frac{W_\mathrm{o}^2}{b^2}\left(\eta_{b1,\theta}\phi_{\mathrm{o}1,r} + \eta_{b1}\phi_{\mathrm{o}1,r\theta} - \frac{2\eta_{b1}\phi_{\mathrm{o}1,\theta}}{b}\right) - \frac{3g_\mathrm{o}W_\mathrm{o}^2\eta_{b1}^2}{2b^4} \\
&\qquad + \frac{1}{2}\left(\phi_{\mathrm{L}1,x}^2 + \phi_{\mathrm{L}1,r}^2 + \frac{\phi_{\mathrm{L}1,\theta}^2}{b^2}\right) - \frac{1}{2}g_\mathrm{o}\left(\phi_{\mathrm{o}1,x}^2 + \phi_{\mathrm{o}1,r}^2 + \frac{\phi_{\mathrm{o}1,\theta}^2}{b^2}\right) - \frac{(2\eta_{b1}^2 + 4\eta_{b1}\eta_{b1,\theta\theta} - \eta_{b1,\theta}^2 - b^2\eta_{b1,x}^2)}{2We_\mathrm{L}b^3} \quad \text{at } b.
\end{aligned} \tag{26}$$

Initial conditions:

$$\eta_{a2}(x,\theta,0) = 0 \quad \text{and} \quad \eta_{a2,t}(x,\theta,0) = 0, \tag{27}$$

$$\eta_{b2}(x,\theta,0) = 0 \quad \text{and} \quad \eta_{b2,t}(x,\theta,0) = 0. \tag{28}$$

Solution of the first- and the second-order equations can be obtained by using the method of Laplace transform and require tedious and lengthy manipulations. The solution methodology and the final solutions for the liquid, inner gas, and outer gas velocity potentials as well as the first- and the second-order surface deformations ($\eta_{a1}, \eta_{a2}, \eta_{b1}$ and η_{b2}) are given

in the Appendix. The first- and the second-order dispersion equations are solved using *Mathematica*™. The secant method is used which requires two initial guess values. Using the first- and second-order surface deformation at the two interfaces we obtain the expressions for the evolution of the inner and outer gas–liquid interface:

$$\eta_a(x,\theta,t) = \eta_o^1\eta_{a1} + \eta_o^2\eta_{a2}, \tag{29}$$

$$\eta_b(x,\theta,t) = \eta_o^1\eta_{b1} + \eta_o^2\eta_{b2}. \tag{30}$$

3. Results and discussion

We consider the temporal evolution of an annular liquid sheet in response to a small disturbance imposed on it. The dimensionless surface deformations at the inner and outer liquid–gas interface are plotted and they are given by $r_a = a + \eta_a$ and $r_b = b + \eta_b$, respectively. The sheet is considered to break when the sheet thickness goes to zero. Numerically, this condition is implemented by considering sheet breakup when the dimensionless sheet thickness becomes less than 10^{-6}. Since the equations are solved numerically on a computer and the evolution of the sheet is obtained numerically, a numerical criterion must be defined to decide when the sheet thickness becomes "zero" within the numerical accuracy of the solution. We note that as far as this number is small, less than 1/1000th of the initial disturbance amplitude, it does not make any significant change in the breakup time results. The first-order growth rate is evaluated for all values of disturbance axial wave number. For a liquid sheet moving in a stagnant gas the disturbance growth rate variations for fundamental (first order) and first harmonic (second order) modes are shown in Fig. 2 for liquid Weber number of 80. This dispersion diagram shows that there is a range of wave number which corresponds to non-zero, positive disturbance growth rate. In this case, for the fundamental mode the maximum growth rate corresponds to the axial wave number of 0.045. The growth rate is evaluated for all combinations of axial and circumferential wave numbers beginning with axisymmetric ($n = 0$) and then asymmetric higher helical modes ($\infty > n > 0$) to determine the combination of axial and circumferential wave number that has the highest growth rate. This is the dominant or most unstable disturbance. This most unstable disturbance is imposed on the sheet surface and its temporal evolution is evaluated. When the disturbance amplitude is plotted against the predicted breakup time on a semi-logarithmic scale, a linear relationship emerges as shown in Fig. 3. The slope of the lines provides the "equivalent" growth rate for the nonlinear sheet breakup (Lafrance, 1975).

The initial magnitude of the imposed disturbance must be provided as an input to the model. It is known that the initial disturbance magnitude is a function of flow conditions and atomizer geometry (Mansour and Chigier, 1994; Grant and Middelman, 1966; Blaisot and Adeline, 2000). However there is no unanimity on its value for a given geometry and flow conditions. Mansour and Chigier (1994) have shown that the initial disturbance magnitude is lower for a laminar jet by orders of magnitude compared to that for a turbulent jet. They have reported that the stability dynamics of the jet is not affected by the presence of turbulence but the shorter breakup lengths obtained with turbulent jets are primarily the result of higher initial disturbance magnitudes. For planar liquid sheets, values of 0.1–0.001 have been used in the literature

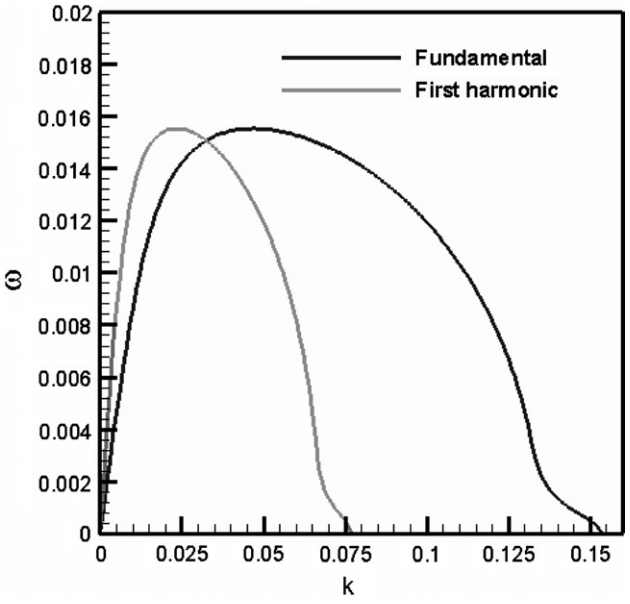

Fig. 2. Growth rate versus axial wave number for the fundamental and the first harmonic modes at $We_L = 80$, $U_i = U_o = 0$, $g_i = g_o = 001$.

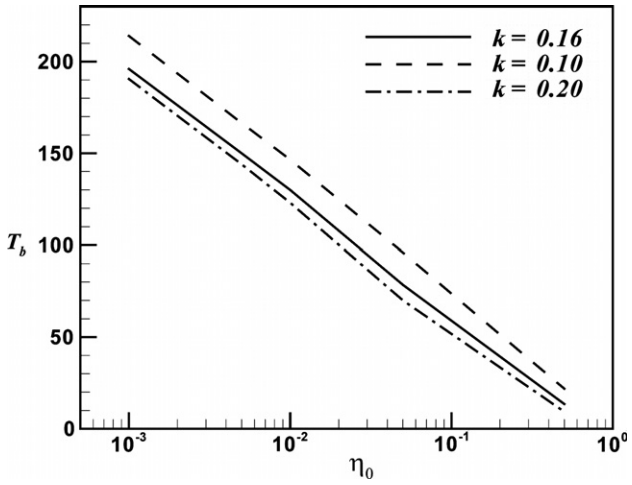

Fig. 3. The variation of breakup time with initial disturbance amplitude which provides effective disturbance growth rate. $We_L = 300$, $U_i = U_o = 0$, and $g_i = g_o = 0.0012$.

(Clark and Dombrowski, 1972; Tharakan et al., 2002; Jazayeri and Li, 2000; Mitra, 2001). Tharakan et al. (2002) found a good agreement between their numerical solutions and their experimental data of planar liquid sheet breakup length with initial magnitude of about 0.1. For the annular sheet breakup investigated here, the dimensionless initial disturbance magnitude is expected to be in the same range as a planar liquid sheet, as such a similar value is used here. It has been shown that the value of the initial disturbance does not change the characteristics of the breakup process and the behavior of the breakup length with liquid and air velocity (Jazayeri and Li, 2000).

3.1. Planar sheet ($a/h \to \infty$)

3.1.1. Mathematical validation

As mentioned earlier, behavior of different sheet/jet geometries can be obtained as limiting cases of the model presented here. This allows us to mathematically validate our model with earlier nonlinear breakup analysis of Clark and Dombrowski (1972). They modeled a planar sheet evolution and breakup in stagnant gas using a perturbation method. Their results can be recovered from our model by increasing the inner radius while keeping the sheet thickness constant. Table 1 shows a comparison of dimensionless breakup time predicted by our model for different values of a/h. It is seen from the results that the curvature effect becomes smaller at high values of a/h and for $a/h = 400$ predicted dimensionless breakup time asymptotically matches those of Clark and Dombrowski's model.

3.1.2. Validation with experimental data

Results of the new model must be compared with experimental data to provide further credence to the model and to ensure that the underlying physics of the process is captured by the analysis. To this end, we have carried out model validation against experimental measurements of planar sheet breakup length obtained by Tharakan et al. (2002). They measured the breakup lengths of planar water sheets of thicknesses 0.3 mm, 0.45 mm and 0.6 mm and width of 20 mm injected in stagnant air. Comparison of our predictions with their experimental data is shown in Table 2 which shows a good agreement and provides validation for our model.

Table 1
Comparison of dimensionless breakup length with planar sheet analysis of Clark and Dombrowski (1972) at different values of dimensionless inner radius

Ratio of inner radius to sheet thickness	Dimensionless breakup time		
	$We = 50$	$We = 100$	$We = 150$
$a/h = 50$	1060	823	663
$a/h = 100$	1390	918	703
$a/h = 200$	1565	953	720
$a/h = 300$	1630	967	725
$a/h = 400$	1640	970	726
Planar sheet ($a/h \to \infty$) Clark and Dombrowski (1972)	1644	971	726

Table 2
Comparison of the dimensionless breakup length with experimental measurements of Tharakan et al. (2002)

Sheet Thickness (mm)	Liquid velocity (m/s)	Dimensionless breakup length (breakup length/sheet thickness)	
		Model prediction	Experimental measurements
0.3	8.14	835	836
	9.25	711	726
0.45	5.86	883	813
	6.79	765	730
0.6	6.49	717	704
	6.96	546	572

3.2. Annular sheet ($0 < a/h < \infty$)

Fig. 4 shows the temporal and spatial evolution of the inner and outer interfaces at axial liquid Weber number of 300 for two wavelength intervals axial distance ($4\pi/k$) at different times. The axial dominant wave number (k) is 0.16 and an initial dimensionless disturbance amplitude (η_0) of 0.1 ($O(10^{-4}$ m)) is considered. The thick solid lines indicate disturbance growth given by a linear analysis and the gray area shows the evolution of the sheet cross-section predicted by the nonlinear model. Initially when the disturbance amplitude is small, the two interfaces appear to move parallel to each other – and follow the behavior predicted by linear analyses. This is to be expected as the disturbance magnitude is very small at short times and provides further validation of the nonlinear model. However, later waviness begins to appear at the interfaces due to the nonlinear interaction between the first- and second-order modes. As the time increases the disturbance amplitude of the inner and

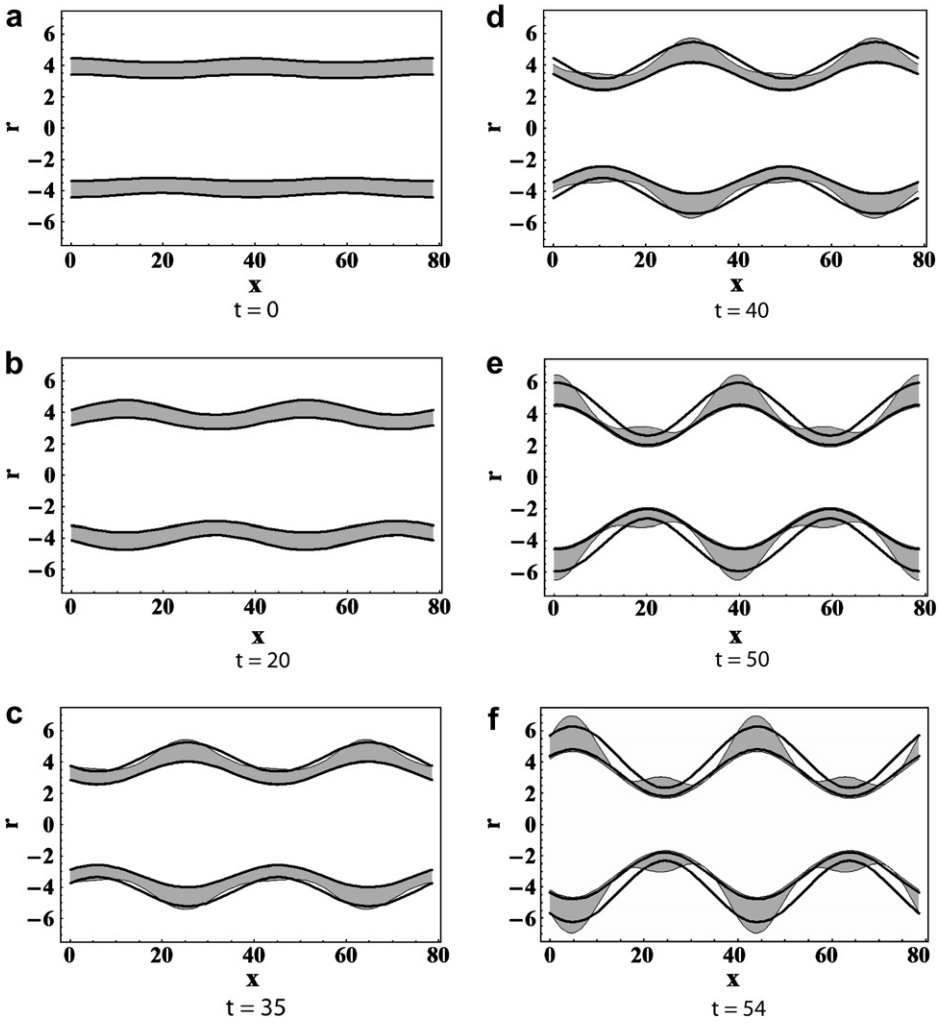

Fig. 4. Temporal evolution of the dimensionless inner and outer surfaces deformation at the dominant wave number of $k = 0.16$. $We_L = 300$, $U_i = U_o = 0$, $g_i = g_o = 0.0012$ ($\eta_o = 0.1$): Thick solid lines indicate linear theory and gray area shows sheet cross-section evolution with nonlinear analysis. (a) $t = 0$, (b) $t = 20$, (c) $t = 35$, (d) $t = 40$, (e) $t = 50$, and (f) $t = 54.5$ (breakup).

outer interfaces increases significantly. The deformation of the inner and outer interfaces leads to thinning and thickening of the liquid sheet. We note that even when sheet deformation becomes very large, the linear theory shows the two interfaces as essentially parallel with virtually no thinning of the sheet and hence linear theory is unable to predict sheet breakup.

It has been shown in the literature that when $\rho_{gas}/\rho_{liquid} < 0.1$ the sinuous mode is the most unstable mode (Mehring and Sirignano, 1999), which is invariably the case in any practical application. For a sinuous disturbance, in the linear treatment for a liquid sheet, both interfaces grow and remain nearly parallel to each other at all times. As seen in Fig. 4, even when the disturbance amplitude becomes large, the distance between the interfaces remains essentially equal to initial sheet thickness, hence no breakup can be directly predicted by a linear theory. The comparison of linear and nonlinear predictions at the time of breakup shown in Fig. 4 illustrates the limitation of the linear theory.

The time at which the thickness of the liquid sheet reaches a near zero value is taken as breakup time. Li (1993) has shown that for liquid Weber numbers much larger than unity the spatial instability of plane liquid sheets is related to the corresponding temporal instability through Gaster's transformation (Gaster, 1964). By replacing the dimensionless time t in Eqs. (29) and (30) by the dimensionless distance x from the injector exit, the temporal development of the disturbance waves on the inner and outer surfaces is transformed into the spatial evolution (Jazayeri and Li, 2000). Such method has been used in the literature (see for example, Jazayeri and Li, 2000). However, it is important to point out the limitations of this approach. Recently, Chuech (2006) made detailed comparison between the temporal and spatial disturbance growth rates for a planar viscous liquid sheet for a range of Weber and Reynolds numbers. He suggests that above $We_L = 100$ the difference between temporal and spatial growth rates is negligible. His plots of results show that at Weber number above 20 there is very little difference between the growth rates predicted by the temporal and the spatial method (less than 1%). However, the difference increases at low Weber numbers. At $We_L = 10$, the difference in the two methods is about 4%, which increases to about 12% at $We_L = 5$ for the cases considered by him. These cases were reported at $Re = 1000$ and it is stated that the difference decreases with increasing Reynolds number. As such the differences in the two methods for present inviscid analysis which corresponds to high Reynolds number may be slightly lower. However the approach of relating temporal and spatial growth rates would be applicable only at high Weber numbers. The spatial evolutions of the inner and outer surfaces for $We_L = 300$ at three different initial disturbance amplitudes of 0.1, 0.01 and 0.001 are shown in Fig. 5. The disturbance waves on the inner and outer surfaces develop at the injector exit and their corresponding amplitudes increases downstream. It can be seen that the disturbance waves remain para-sinuous for most of the annular liquid sheet length. Annular liquid sheet thinning and pinching occur because of the nonlinear effects which lead to the liquid sheet breakup. With increasing the initial disturbance amplitude, the sheet breakup becomes much closer to the injector exit, and the sheet breakup length is reduced.

Further validation of the model is carried out by comparing our predictions with experimental measurements of sheet breakup lengths reported by Shen (1997). Shen investigated the effect of air flow on sheet breakup with a coaxial atomizer with an outer radius of 5 mm which provided liquid sheet of thickness 0.238 mm. Fig. 6 shows the variation of liquid sheet breakup length with gas-to-liquid velocity ratio. With constant liquid velocity, increase in gas-to-liquid velocity ratio indicates higher gas velocity which leads to increased aerodynamic interaction between the gas flow and the liquid. This results in a shorter breakup length with increase in gas-to-liquid velocity ratio. Both our predictions and data from Shen (1997) show this trend. Moreover, there is good agreement between predictions and measurements of breakup length.

As mentioned earlier, due to the inability of the linear theory to predict breakup point for a para-sinuous disturbance, a breakup criterion has been applied with the linear theory where the sheet is considered to break when the disturbance is grown by a factor e^N. Clark and Dombrowski (1972) suggested $N = 12$, although one would expect this factor to depend on the initial disturbance amplitude. In Table 3 below we have compared calculated values of N based on a linear theory from breakup length predictions using the nonlinear model for different values of the liquid to gas velocity ratio. It is seen that there no unanimity of value for N at all gas-to-liquid velocity ratios.

3.2.1. Comparison between the inner and the outer gas flow

The effect of gas–liquid velocity ratio on the ligament shape and the breakup time is presented in Figs. 7a–c. The breakup time and axial wave number for only inner gas are 25 and 0.39, respectively (Fig. 7a). The breakup time and axial wave number for both inner and outer gas streams are 11.5 and 0.7, respectively (Fig. 7c). The corresponding case of sheet breakup in stagnant gas is shown in Fig. 4 and has breakup time of 54.5 and the axial wave number of 0.16. It can be seen in Fig. 7 that the ligament shape and size during breakup process are different in the three cases. In the case of only outer gas stream, the ligament shape is similar to liquid jet breakup in Rayleigh regime where the jet is known to breakup with large main drop followed by smaller satellite drop. This is similar to findings of Panchagnula et al. (1998) who reported that the annular sheet breaks up into a main ring followed by a satellite ring at low liquid Weber numbers. With increasing axial gas–liquid velocity ratio, the maximum growth rate increases and leads to shorter breakup length which has been seen in experimental measurements reported by Carvalho and Heitor (1998) and Lavergne et al. (1993). The more uniform ligament sizes obtained when both inner and outer flows are present, may explain the narrower drop size distribution reported in Shen (1997) with inner and outer gas flow.

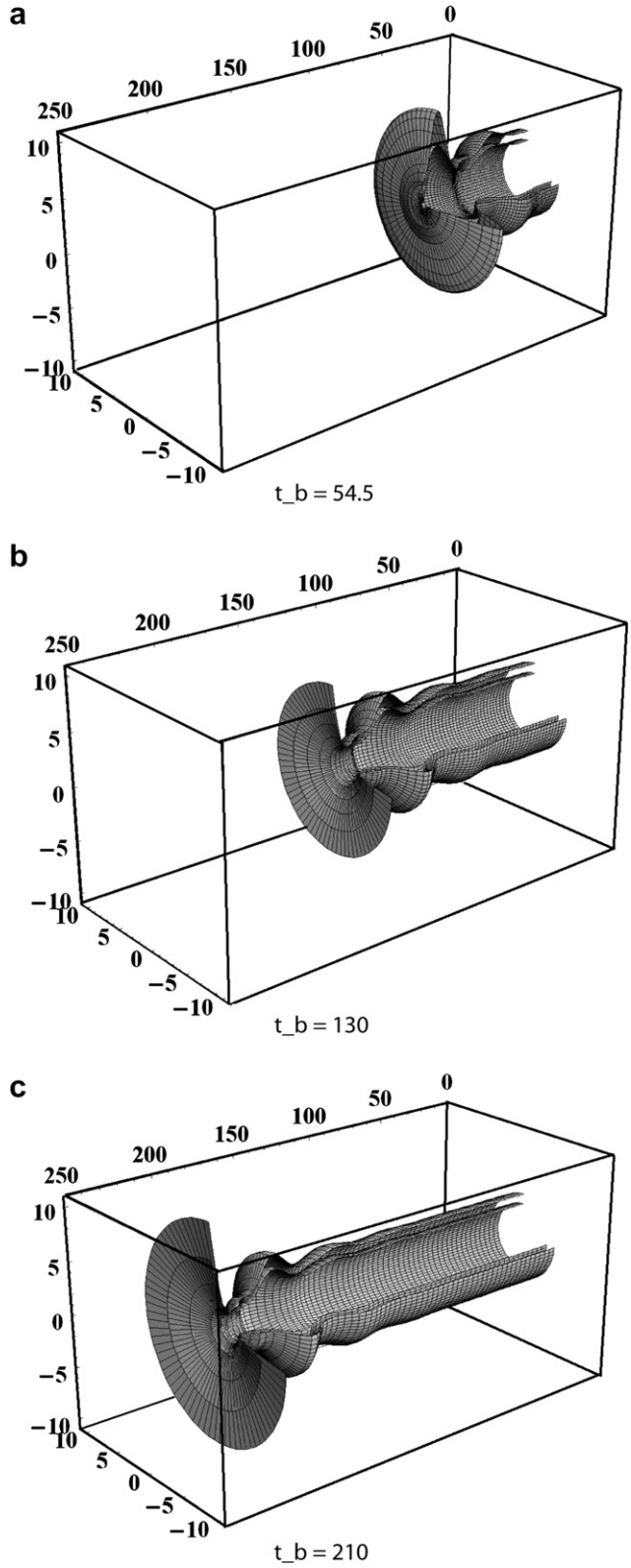

Fig. 5. Spatial evolution of inner and outer surface deformations at different initial disturbance amplitudes for $We_L = 300$, $U_i = U_o = 0$, $g_i = g_o = 0.0012$ and $k = 0.16$. (a) $\eta_o = 0.1$, $t_b = 54.5$, (b) $\eta_o = 0.01$, $t_b = 130$, and (c) $\eta_o = 0.001$, $t_b = 210$.

The variation of sheet breakup time with gas-to-liquid velocity ratio is plotted in Fig. 8 for only inner gas flow, only outer gas flow, and when both gas flows are present. It is clear by comparing Figs. 4 and 8 that inner or outer or both inner and outer gas flow decreases the breakup time and increases the axial wave number. The maximum disturbance growth rate of only inner axial gas stream is larger than that of only outer axial air stream. This indicates that axial inner gas stream is more

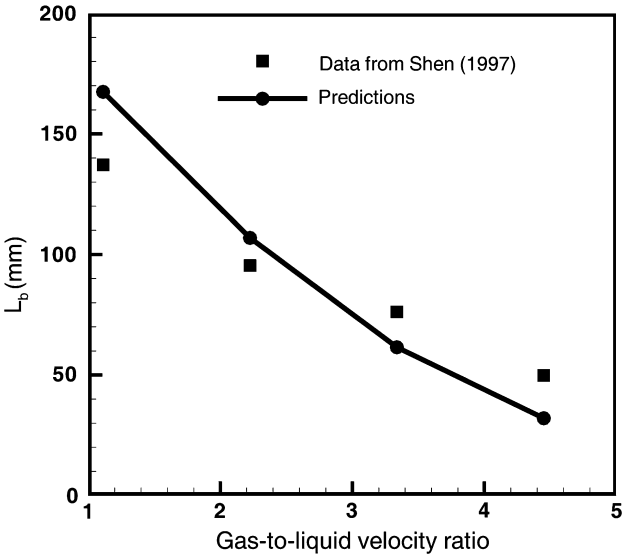

Fig. 6. Comparison of predicted breakup length with data from Shen (1997) for different gas-to-liquid velocity ratios.

Table 3
Values of N for linear breakup criterion e^N for $We_L = 38.5$, $r_a = 20.05263$, and $r_b = 21.05263$

Gas-to-liquid velocity ratio	Dimensionless growth rate	N
1.11	0.009427819	5.44
2.22	0.015428413	6.48
3.33	0.026721457	6.41
4.45	0.042337323	5.42

effective than outer axial gas stream in enhancing the instability of annular liquid sheets. Such effectiveness of inner gas stream over outer gas stream has been demonstrated in experimental observations of Adzic et al. (2001). Both inner and outer axial gas streams case has the largest disturbance growth rate compared to only inner gas stream and only outer gas stream because with the presence of both inner and outer axial gas streams, the disturbance extracts energy from both the inner and the outer axial gas flow.

3.2.2. Effect of outer gas swirl

Fig. 9 presents the dimensionless inner and outer surfaces deformation at the time of breakup for different outer gas swirl strength values ($W_o = 0$, 70, 100 and 210) for $We_L = 4$, $U_i = 0$ and $U_o = 15$. In the absence of outer gas swirl, the maximum growth rate of the axisymmetric mode ($n = 0$) is higher than that of the helical modes. This is not surprising as the base flow in this case is axisymmetric and the outer gas stream moves perpendicular to the circumferential direction. As such the primary aerodynamic interaction is in the axial direction and makes the axisymmetric mode as the most dominant mode. The breakup time for no gas swirl case is 56.5 for axial (k) and circumferential (n) wave numbers of 0.26 and zero, respectively (Fig. 9a). It can be observed from that outer gas swirl not only increases the growth rate and the range of unstable wave numbers but also shifts the dominant mode from the axisymmetric mode ($n = 0$) to a helical mode ($n > 0$). This in agreement with the experimental investigations of Carvalho and Heitor (1998), Chin et al. (2000) and He et al. (2003). As swirl is added to the outer air flow, the pressure increases outward from the sheet surface and the positive radial pressure gradient of the base flow decreases the growth rate of the axisymmetric mode. However, the swirl velocity increases the growth rate of the asymmetric (helical) mode ($n > 0$). As the swirl strength increases, the most unstable disturbance wavelength becomes smaller (i.e. the most unstable circumferential wave number become larger). For outer gas swirling strength of 70, the optimal disturbance growth rate occurs at the third helical mode ($n = 3$). For outer gas swirl strength (W_o) of 210, the most unstable circumferential wave number (n) reaches a value of 14. Also, the growth rate of the most unstable disturbance is much higher at higher swirl strength. Consequently, when the outer gas swirl strength increases from 0 to 210 the dimensionless breakup time decreases from 56.5 to 14.75. It can be seen that the outer gas swirl strength speeds up the breakup process of the annular liquid sheet. If we compare Figs. 9b and d, we can clearly see that the ligaments become thinner with increasing gas swirl strength. Fig. 10 shows the spatial plot of the inner and outer surface deformation for two different outer gas swirl strength values. For both cases, the breakup is highly asymmetric. As the

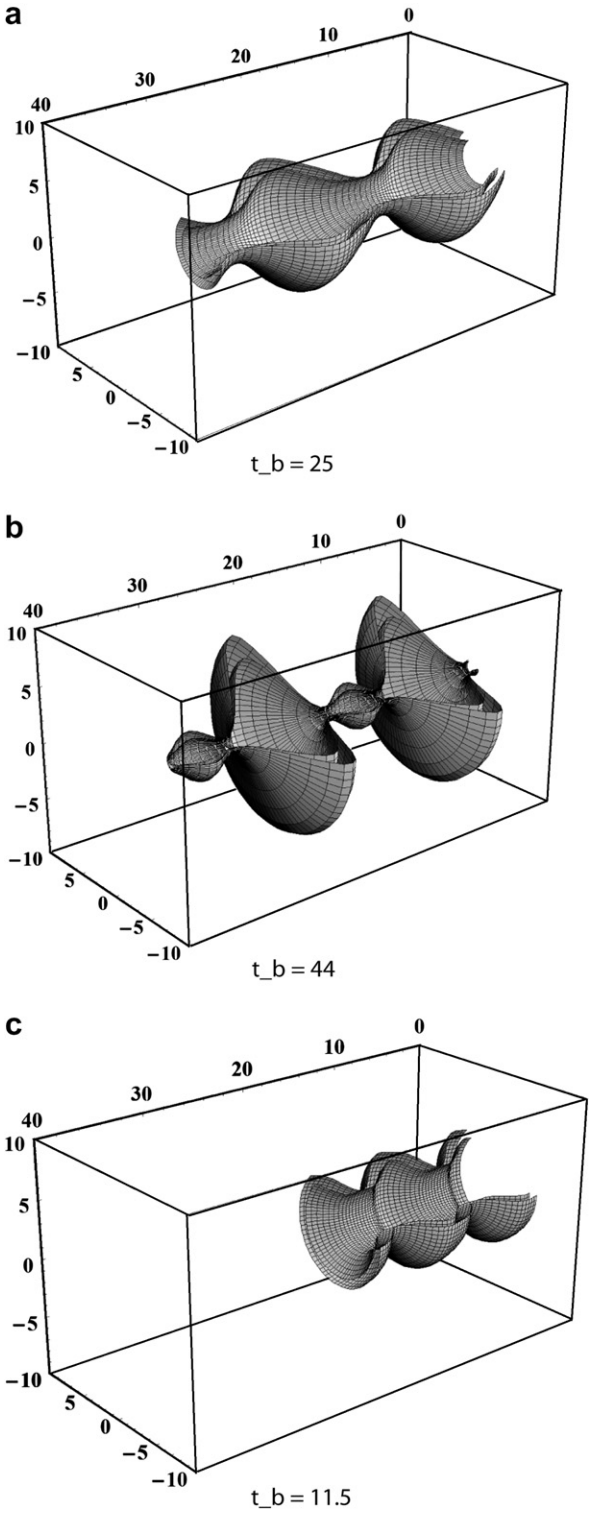

Fig. 7. Inner and outer surface deformation at the time of breakup for different inner and outer gas–liquid velocity ratios for $We_L = 300$, $g_i = g_o = 0.0012$, and $\eta_o = 0.1$: (a) $U_i = 3$, $U_o = 0$, and $k = 0.39$, $t_b = 25$, (b) $U_i = 0$, $U_o = 3$, $t_b = 44$, and $k = 0.37$, and (c) $U_i = U_o = 3$, $t_b = 11.5$, and $k = 0.7$.

outer gas swirl strength increases from 50 to 100, the breakup time decreases from 46.5 to 34.67. The net effect of outer gas swirl is three-fold. First, the outer gas swirl changes the most unstable disturbance from axisymmetric to higher helical mode, which leads to a highly asymmetric breakup. Second, the most unstable circumferential wave number increases with increasing swirl strength and produces thinner ligaments which are likely to result in smaller droplet sizes. Third, due to increase in the growth rate of the most unstable disturbance with increasing swirl strength, the breakup length decreases significantly. These findings are consistent with the experimental observations of Carvalho and Heitor (1998).

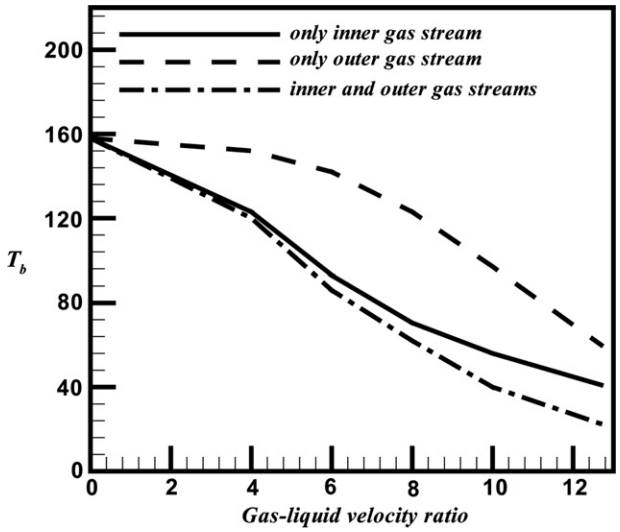

Fig. 8. Effect of gas–liquid velocity ratio on the breakup time $We_L = 4$, $g_i = g_o = 0.0012$.

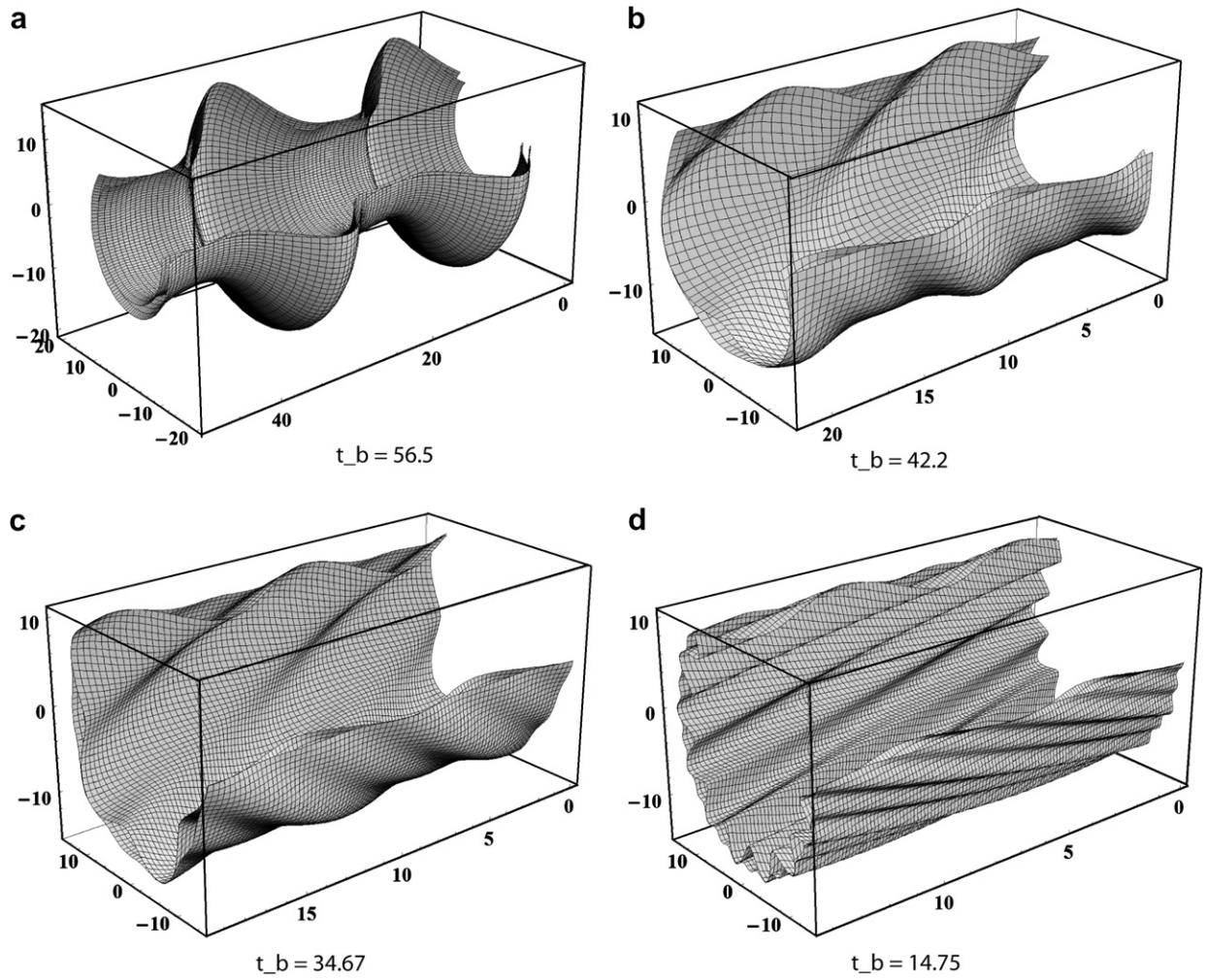

Fig. 9. Dimensionless surface deformation at the time of breakup for different outer gas swirl strength values for $We_L = 4$, $U_i = 0$, $U_o = 15$, $g_i = g_o = 0.0012$ and $\eta_o = 0.001$: (a) $W_o = 0$, $n = 0$, $t_b = 56.5$, (b) $W_o = 70$, $n = 3$, $t_b = 42.2$, (c) $W_o = 100$, $n = 5$, $t_b = 34.67$, and (d) $W_o = 210$, $n = 14$, $t_b = 14.75$.

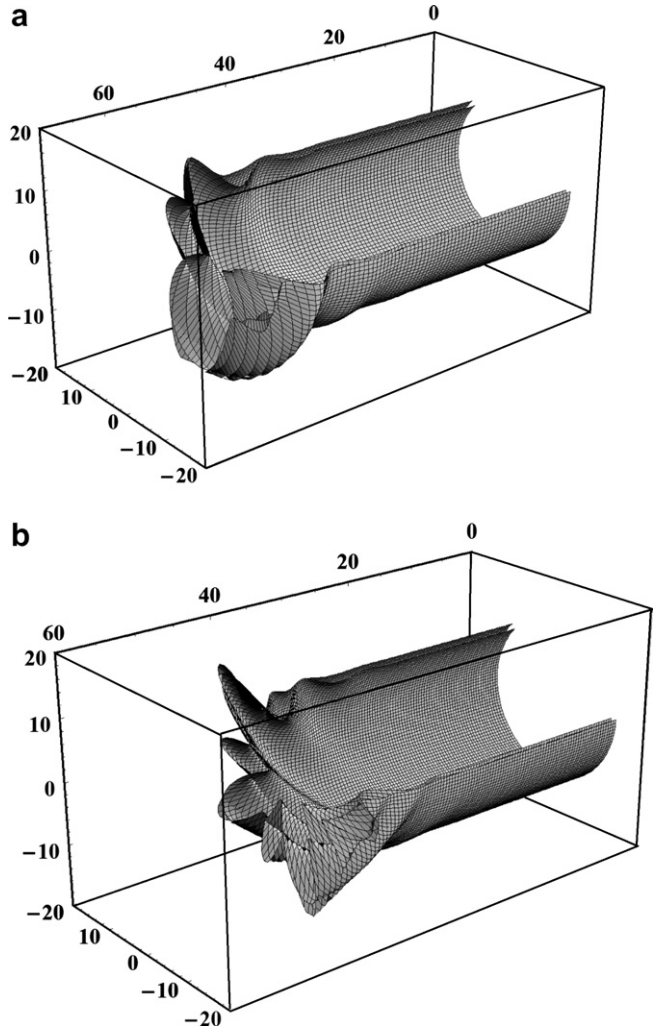

Fig. 10. Spatial evolution of the dimensionless surface deformation at different gas swirl strength values for $We_L = 4$, $U_i = 0$, $U_o = 15$, $g_i = g_o = 0.0012$ and $\eta_o = 0.001$. (a) $W_o = 50$, $n = 2$ and (b) $W_o = 100$, $n = 5$.

3.3. Jet breakup ($a/h = 0$)

3.3.1. Effect of gas swirl

The influence of gas swirl on the maximum disturbance growth rate for limiting case of a coaxial jet ($a/h = 0$) is shown in Fig. 11 for axial gas-to-liquid velocity ratio $U_o = 10$ and $We_L = 6$ for different circumferential modes. Fig. 11 shows that at very low gas swirl strength (gas swirl-to-axial velocity ratio < 0.5), the axisymmetric mode ($n = 0$) has the highest maximum growth rate. As the gas swirl number is increased, the growth rate of the axisymmetric mode decreases. The decrease in the growth rate of the axisymmetric disturbance is caused by the radial static pressure variation in the swirling gas stream. The gas pressure increases radially outwards from the jet surface in a swirling gas stream and tends to produce a stabilizing effect on axisymmetric disturbances. However, as the gas swirl velocity increases, the aerodynamic effect on the helical disturbances becomes increasingly dominant and their growth rate increases. At the gas swirl-to-axial velocity ratio of about 0.5, the disturbance growth rate of the first helical mode exceeds that of the axisymmetric mode. The second transition point is reached at gas swirl-to-axial ratio of about 2 where the growth rate of the second helical mode is greater than that of the first helical mode. With increasing swirl velocity, the maximum growth rate of the higher helical disturbance modes increases significantly. Therefore, at high swirl velocity, the most unstable mode will be a higher helical mode and a large growth rate which will break the jet in several circumferential fragments and the breakup length will decrease with increasing swirl velocity. This behavior is in line with experimental observations (Hopfinger and Lasheras (1996) and Dunand et al. (2005)). Earlier linear analyses of Lian and Lin (1990), Liao et al. (2000a) and Lin (2003) have predicted that axisymmetric mode is the most dominant mode in presence of gas swirl and gas swirl has a stabilizing influence on the jet. Our results contradict earlier linear theories and capture the destabilizing behavior of gas swirl observed in experiments.

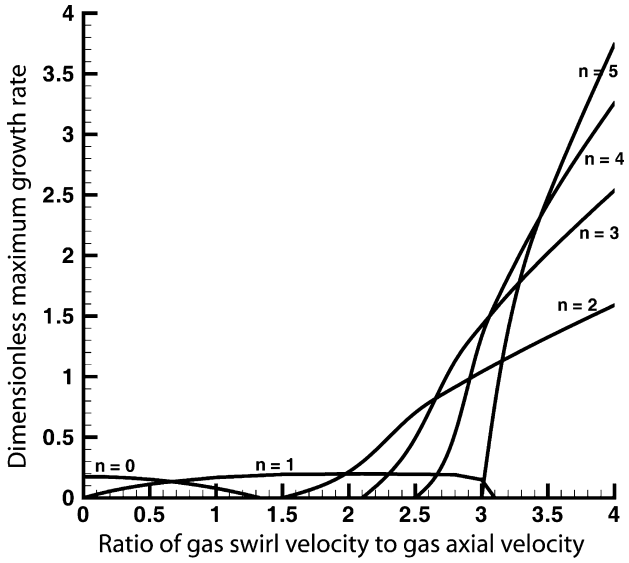

Fig. 11. Maximum disturbance growth rate versus gas swirl-to-axial velocity ratio for axisymmetric and helical modes. $U_o = 10$ and $We_L = 6$.

3.4. Summary and conclusions

A three-dimensional nonlinear temporal instability analysis has been carried out to model the breakup of an annular liquid sheet. A perturbation expansion technique has been used to model the nonlinear breakup using the initial amplitude of the disturbance as the perturbation parameter. The model is used to determine the evolution of the inner and outer interface up to sheet breakup in response to a small disturbance imposed on it. Also, the breakup of a planar sheet and a coaxial jet is investigated as two limiting cases of the developed model. The effects of liquid Weber number, initial disturbance amplitude, ratio of inner gas velocity to liquid velocity, ratio of outer-gas velocity to liquid velocity and outer air swirl strength on the breakup time is investigated. From this study, we can draw the following conclusions:

1. The developed model can be used to predict breakup length not only for an annular sheet but also for a planar sheet and a jet as limiting cases of $a/h \to \infty$ and $a/h = 0$, respectively.
2. For an annular sheet, even when sheet deformation becomes very large, linear theory shows that the two interfaces deform essentially parallel to each other. As such a linear theory can not predict sheet breakup. Nonlinear treatment is necessary to predict the breakup length for an annular liquid sheet.
3. The axial inner gas stream is found to be more effective in disintegrating and enhancing the instability of an annular liquid sheet than the axial outer gas stream. Presence of both gas streams is more effective in sheet breakup than only one gas stream. Also, when both gas flows are present, more uniform ligaments are obtained compared to only one gas stream. This may explain the narrower droplet distribution obtained with inner and outer gas flow by Shen (1997).
4. When outer air swirl is absent, the axisymmetric mode ($n = 0$) dominates the breakup process of the annular liquid sheet. Outer air swirl promotes the instability of the liquid sheet and switches the dominant mode from the axisymmetric mode to a helical mode ($n > 0$). As outer air swirl strength increases, the circumferential wave number (n) increases, the breakup process becomes highly asymmetric, size of the ligaments decreases and the breakup length shortens significantly.
5. For a limiting case of a coaxial jet ($a/h = 0$), gas swirl is shown to destabilize the jet by changing the dominant mode from axisymmetric to helical and significantly increasing its growth rate. This behavior obtained by the nonlinear model not only agrees well with experimental observations but also contradicts earlier linear analyses of coaxial jets available in literature which predict a stabilizing effect of gas swirl.

Acknowledgements

We thankfully acknowledge the support of this work by University Research Council of University of Cincinnati and GE Transportation Systems.

Appendix. Solution of first- and second-order equations

The first-order surface deformation at the two interfaces can be written in the following form:

$$\eta_{a1}(x,\theta,t) = A_1(t)\exp(\mathrm{i}(kx+n\theta)) + \text{c.c.}, \tag{31}$$
$$\eta_{b1}(x,\theta,t) = B_1(t)\exp(\mathrm{i}(kx+n\theta)) + \text{c.c.}, \tag{32}$$

where c.c. indicates complex conjugate. Substituting these in the governing equations for the first order and solving using the method of Laplace transform we find

$$A_1(t) = \sum_{j=1}^{j=4} c_{1j}a_{1j}\exp(\omega_{1j}t), \tag{33}$$
$$B_1(t) = \sum_{j=1}^{j=4} c_{1j}b_{1j}\exp(\omega_{1j}t). \tag{34}$$

The disturbance growth rates ω_{11}, ω_{12}, ω_{13} and ω_{14} are the roots of the first-order dispersion equations

$$\Delta_{11}\omega_{1j}^4 + \Delta_{12}\omega_{1j}^3 + \Delta_{13}\omega_{1j}^2 + \Delta_{14}\omega_{1j} + \Delta_{15} = 0, \quad j = 1,2,3 \text{ and } 4. \tag{35}$$

The expressions for c_{1j} and Δ_{1j} are available in Ibrahim (2006) and not repeated here for sake of brevity.

The first-order surface deformations are

$$\eta_{a1}(x,\theta,t) = (c_{11}\exp(\omega_{11}t) + c_{12}\exp(\omega_{12}t))\exp(\mathrm{i}(kx+n\theta)) + \text{c.c.}, \tag{36}$$
$$\eta_{b1}(x,\theta,t) = (R(c_{11}\exp(\omega_{11}t) + c_{12}\exp(\omega_{12}t)))\exp(\mathrm{i}(kx+n\theta)) + \text{c.c.}, \tag{37}$$
$$c_{11} = \frac{\omega_{12}}{2(\omega_{12}-\omega_{11})} \quad \text{and} \quad c_{12} = \frac{-\omega_{11}}{2(\omega_{12}-\omega_{11})}, \tag{38}$$
$$\omega_{11} = \alpha - \mathrm{i}\beta, \quad \omega_{12} = -\alpha - \mathrm{i}\beta.$$

The first-order liquid, inner and outer gas velocity potentials are, respectively,

$$\phi_{\mathrm{L1}} = \left[\frac{c_{11}}{2}(f_1(r)m_5 + f_2(r)Rm_8)\exp(\omega_{11}t) + \frac{c_{12}}{2}(f_1(r)m_6 + f_2(r)Rm_9)\exp(\omega_{12}t)\right]\exp(\mathrm{i}(kx+n\theta)) + \text{c.c.}, \tag{39}$$
$$\phi_{\mathrm{i1}} = \left[f_3(r)\left(\frac{c_{11}}{2}m_{17}\exp(\omega_{11}t) + \frac{c_{12}}{2}m_{18}\exp(\omega_{12}t)\right)\right]\exp(\mathrm{i}(kx+n\theta)) + \text{c.c.}, \tag{40}$$
$$\phi_{\mathrm{o1}} = \left[f_4(kr)R\left(\frac{c_{11}}{2}m_{23}\exp(\omega_{11}t) + \frac{c_{12}}{2}m_{24}\exp(\omega_{12}t)\right)\right]\exp(\mathrm{i}(kx+n\theta)) + \text{c.c.} \tag{41}$$

Similarly the second-order surface deformation at the two interfaces can be written in the following form:

$$\eta_{a2}(x,\theta,t) = A_2(t)\exp(2\mathrm{i}(kx+n\theta)) + \text{c.c.} + D_a(t), \tag{42}$$
$$\eta_{b2}(x,\theta,t) = B_2(t)\exp(2\mathrm{i}(kx+n\theta)) + \text{c.c.} + D_b(t), \tag{43}$$

where

$$A_2(t) = c_{1a}\exp(\omega_{21}t) + c_{2a}\exp(\omega_{22}t) + c_{3a}\exp(2\omega_{11}t) + c_{4a}\exp(2\omega_{12}t) + c_{5a}\exp((\omega_{11}+\omega_{12})t), \tag{44}$$
$$B_2(t) = c_{1b}\exp(\omega_{21}t) + c_{2b}\exp(\omega_{22}t) + c_{3b}\exp(2\omega_{11}t) + c_{4b}\exp(2\omega_{12}t) + c_{5b}\exp((\omega_{11}+\omega_{12})t). \tag{45}$$

$D_a(t)$ and $D_b(t)$ are required to insure a conservation of mass at $t > 0$. Substituting these in Eq. (20), we find that

$$D_a(t) = \frac{(k^2 f_3 + \frac{n^2}{a^2}f_3 - f_3'')(\alpha^2+\beta^2)}{8\alpha^2}(1-\cosh(2\alpha t)), \tag{46}$$
$$D_b(t) = \frac{(k^2 f_4 + \frac{n^2}{b^2}f_4 - f_4'')(\alpha^2+\beta^2)}{8\alpha^2}(1-\cosh(2\alpha t)). \tag{47}$$

Following a similar procedure to the one described for the first-order solution, after lengthy and tedious manipulations, the second-order liquid, inner and outer gas velocity potentials can be obtained as follows:

$$\phi_{L2} = [(f_5(r)c_{1a}m_1 + f_6(r)c_{1b}m_3)\exp(\omega_{21}t) + (f_5(r)c_{2a}m_2 + f_6(r)c_{2b}m_4)\exp(\omega_{22}t) + (f_5(r)(c_{3a}m_5 - m_{11}) + f_6(r)(c_{3b}m_8 - m_{14}))\exp(2\omega_{11}t) + (f_5(r)(c_{4a}m_6 - m_{12}) + f_6(r)(c_{4b}m_9 - m_{15}))\exp(2\omega_{12}t) + (f_5(r)(c_{5a}m_7 - m_{12}) + f_6(r)(c_{5b}m_{10} - m_{16}))\exp((\omega_{11} + \omega_{12})t)]\exp(2i(kx + n\theta)) + \text{c.c.}, \quad (48)$$

$$\phi_{i2} = [f_7(r)c_{1a}m_{29}\exp(\omega_{21}t) + f_7(r)c_{2a}m_{30}\exp(\omega_{22}t) + (f_7(r)(c_{3a}m_{17} - m_{20}))\exp(2\omega_{11}t) + (f_7(r)(c_{4a}m_{18} - m_{21}))\exp(2\omega_{12}t) + (f_7(r)(c_{5a}m_{19} - m_{22}))\exp((\omega_{11} + \omega_{12})t)]\exp(2i(kx + n\theta)) + \text{c.c.} + A_i(t) \quad (49)$$

$$\phi_{o2} = [f_8(r)c_{1b}m_{31}\exp(\omega_{21}t) + f_8(r)c_{2b}m_{32}\exp(\omega_{22}t) + (f_8(r)(c_{3b}m_{23} - m_{26}))\exp(2\omega_{11}t) + (f_8(r)(c_{4b}m_{24} - m_{27}))\exp(2\omega_{12}t) + (f_8(r)(c_{5b}m_{25} - m_{28}))\exp((\omega_{11} + \omega_{12})t)]\exp(2i(kx + n\theta)) + \text{c.c.} + A_o(t), \quad (50)$$

where $A_i(t)$ and $A_o(t)$ are required to satisfy the dynamic boundary conditions. Substitution of theses velocity potentials into the second-order dynamic boundary condition and the initial conditions yields the above time dependent terms. After considerable amount of manipulations, the following equations for the second-order growth rate are obtained:

$$\Delta_{21}\omega_{2j}^4 + \Delta_{22}\omega_{2j}^3 + \Delta_{23}\omega_{2j}^2 + \Delta_{24}\omega_{2j} + \Delta_{25} = 0, \quad j = 1, 2, 3 \text{ and } 4. \quad (51)$$

The expressions for constants in the above equations ($c_{1a} - c_{5a}, c_{1b} - c_{5b}, m_1 - m_{22}, \Delta_{2j}$) and functions ($f_1 - f_8$) are available in Ibrahim (2006).

References

Adzic, M., Carvalho, I.S., Heitor, M.V., 2001. Visualization of the disintegration on an annular liquid sheet in a coaxial airblast injector at low atomizing air velocities. Opt. Diag. Eng. 5, 27–38.

Alleborn, N., Raszillier, H., Durst, F., 1998. Linear stability of non-Newtonian annular liquid sheets. Acta Mech. 137, 33–42.

Arai, T., Hashimoto, H., 1985. In: Proceedings of the 3rd International Conference on Liquid Atomization and Spray Systems, London, VIB/1/1-7.

Blaisot, J.B., Adeline, S., 2000. Determination of the growth rate of instability of low velocity free falling jets. Exp. Fluids 29, 247–256.

Blaisot, J.B., Adeline, S., 2003. Instabilities on a free falling jet under an internal flow breakup mode regime. Int. J. Multiphase Flow 29, 629–653.

Cao, J., 2003. Theoretical and experimental study of atomization from an annular liquid sheet. J. Automobile Eng. 217, 734–735.

Carvalho, I.S., Heitor, M.V., 1998. Liquid film break-up in a model of a prefilming airblast nozzle. Exp. Fluids 24, 408–415.

Chin, J.S., Rizk, N.K., Razan, M.K., 2000. Effect of inner and outer air flow characteristics on high liquid pressure prefilming airblast atomization. J. Prop. Power 16, 297–301.

Chuech, S.G., 2006. Spatial Instability of A viscous Liquid sheet. Int. J. Numer. Meth. Fluids 50, 1461–1474.

Clark, C.J., Dombrowski, N., 1972. Aerodynamic instability and disintegration of inviscid liquid sheets. Proceeding of Royal Society London A 329, 467–478.

Cousin, J., Dumouchel, C., 1996. The effect of viscosity on the linear instability of a flat liquid sheet. Atomization Sprays 6, 563–576.

Du, Q., Li, X., 2005. Effect of gas stream swirls on the instability of viscous annular liquid jets. Acta Mech. 176, 61–81.

Dunand, A., Carreau, J.L., Roger, F., 2005. Liquid jet breakup and atomization by annular swirling gas jet. Atomization Sprays 15, 223–247.

Eroglu, H., Chigier, N., Farago, Z.Z., 1991. Coaxial atomizer liquid intact lengths. Phys. Fluids A3, 303–308.

Gaster, M., 1964. A note on the relation between temporally-increasing and spatially-increasing disturbances in hydrodynamic stability. J. Fluid Mech. 14, 222–224.

Grant, R.P., Middelman, S., 1966. Newtonian jet stability. AIChE J. 12, 669–673.

He, W.Z., Jiang, Z.H., Suo, Q.L., 2003. Analysis of energy efficiency of air in atomizing pseudoplastic liquid using a specially designed prefilming airblast atomizer. Ind. Eng. Chem. Res. 42, 3144–3149.

Hopfinger, E.J., Lasheras, J.C., 1996. Explosive breakup of a liquid jet by a swirling coaxial gas jet. Phys. Fluids 8, 1696–1698.

Ibrahim, A.A., 2006. Comprehensive Study of Internal Flow Field and Linear and Nonlinear Instability of an Annular Liquid Sheet Emanating from an Atomizer. Ph. D. Disseration, University of Cincinnati, Department of Mechanical, Industrial, and Nuclear Engineering.

Ibrahim, A.A., Jog, M.A., 2006. Effect of liquid and air swirl strength and relative rotational direction on the instability of an annular liquid sheet. Acta Mech. 186, 113–133.

Ibrahim, A.A., Jog, M.A., Jeng, S.M., 2006. Effect of liquid swirl velocity profile on the instability of a swirling annular liquid sheet. Atomization Sprays 16, 237–263.

Jazayeri, S.A., Li, X., 2000. Nonlinear instability of plane liquid sheets. J. Fluid Mech. 406, 281–308.

Jeandel, X., Dumouchel, C., 1999. Influence of the viscosity on the linear stability of an annular liquid sheet. Int. J. Heat Fluid Flow 20, 499–506.

Lafrance, P., 1975. Nonlinear breakup of a laminar liquid jet. Phys. Fluids 18, 428–432.

Lavergne, G., Trichet, P., Hebrard, P., Biscos, Y., 1993. Liquid sheet disintegration and atomization process on a simplified airblast atomizer. J. Eng. Gas Turbines Power 115, 461–466.

Lee, C.P., Wang, T.G., 1986. A theoretical model for annular jet instability. Phys. Fluids, 2076–2085.

Lefebvre, A.H., 1980. Airblast atomization. Prog. Energy Combust. Sci. 6, 233–261.

Lefebvre, A.H., Gas Turbine Combustion, Hemisphere, Washington, DC, 1983.

Lefebvre, A.H., Atomization and Sprays, Hemisphere, Washington, DC, 1989.

Li, X., 1993. Spatial instability of plane liquid sheets. Chem. Eng. Sci. 48, 2973–2981.

Lian, Z.W., Lin, S.P., 1990. Breakup of a liquid jet in a swirling gas. Phys. Fluids 2, 2134–2139.

Liao, Y., Jeng, S.M., Jog, M.A., Benjamin, M.A., 2000a. Effect of air swirl profile on the instability of a viscous liquid jet. J. Fluid Mech. 424, 1–20.

Liao, Y., Jeng, S.M., Jog, M.A., Benjamin, M.A., 2000b. Instability of an annular liquid sheet surrounded by swirling airstreams. AIAA J. 38, 453–460.

Liao, Y., Jeng, S.M., Jog, M.A., Benjamin, M.A., 2001. Advanced sub-model for airblast atomizers. J. Prop. Power 17, 411–417.

Lin, S.P., 2003. Breakup of Liquid Sheets and Jets. Cambridge University Press, Cambridge, UK.

Mansour, A., Chigier, N., 1994. Effect of the turbulence on the stability of liquid jets and the resulting droplet size distributions. Atomization Sprays 4, 583–593.

Mehring, C., Sirignano, W.A., 1999a. Axisymmetric capillary waves on thin annular liquid sheets part I: temporal stability. Phys. Fluids 12, 1417–1439.

Mehring, C., Sirignano, W.A., 1999b. Axisymmetric capillary waves on thin annular liquid sheets part II: spatial stability. Phys. Fluids 12, 1440–1460.

Mitra, S.K., 2001. Breakup Process of Plane Liquid Sheets and Prediction of Initial Droplet Size and Velocity Distributions in Sprays, Ph.D. dissertation, University of Waterloo, Faculty of Engineering, Mechanical Engineering Department.

Panchagnula, M.V., Sojka, P.E., Santangelo, P.J., 1996. On the three-dimensional instability of a swirling, annular, inviscid liquid sheet subject to unequal gas velocities. Phys. Fluids 8, 3300–3312.

Panchagnula, M.V., Sojka, P.E., Bajaj, A.K., 1998. The non-linear breakup of annular liquid sheets. Proc. 11th Ann. Conf. Liquid Atom. Spray Systems, 170–174.

Park, H., Heister, S.D., 2006. Nonlinear simulation of free surfaces and atomization in pressure swirl atomizers. Phys. Fluids 18, 052103.

Park, H., Yoon, S.S., Heister, S.D., 2006. On the nonlinear stability of a swirling liquid jet. Int. J. Multiphase Flow 32, 1100–1109.

Ponstein, J., 1959. Instability of rotating cylindrical jets. Appl. Sci. Res. A8, 425–456.

Schmidt, D.P., Chiappetta, L., Goldin, G., Madhabushi, R., 2003. Transient multidimensional modeling of airblast atomizers. Atomization Sprays 13, 364–385.

Shen, J., 1997. Formation and Characteristics of Sprays from Annular Viscous Liquid Jet Breakup. Ph.D. Thesis, University of Victoria, Victoria, BC, Canada.

Shen, J., Li, X., 1996. Instability of an annular viscous liquid jet. Acta Mech. 114, 167–183.

Sirignano, W.A., Mehring, C., 2000. Review of theory of distortion and disintegration of liquid streams. Prog. Energy Comb. Sci. 26, 609–655.

Tharakan, T.J., Ramamurthi, K., Balakrishnan, M., 2002. Nonlinear breakup of thin liquid sheets. Acta Mech. 156, 29–46.

White, F.M., 1991. Viscous Fluid Flow. McGraw-Hill Inc., New York.

Yoon, S.S., Heister, S.D., 2003. Categorizing linear theories for atomizing jets. Atomization Sprays 13, 499–516.

Yoon, S.S., Heister, S.D., 2004. A nonlinear atomization model based on a boundary layer instability mechanism. Phys. Fluids 16, 47–61.